Doubling Exponent Models for the Analysis of Porous Film Electrodes by Impedance. Relaxation of TiO_2 Nanoporous in Aqueous Solution

Juan Bisquert,*,† Germà Garcia-Belmonte,† Francisco Fabregat-Santiago,† Noemí S. Ferriols,† Peter Bogdanoff,‡ and Ernesto C. Pereira§

Departament de Ciències Experimentals, Universitat Jaume I, 12080 Castelló, Spain; Department Solare Energetik, Hahn-Meitner Institut, Glienicker Strasse 100, 14109 Berlin, Germany; and Departamento de Química, Universidade Federal de São Carlos, P.O. Box 676, 13560-905 São Carlos, SP Brazil

Received: September 7, 1999; In Final Form: December 21, 1999

The paper is concerned with the small signal ac impedance of porous film electrodes in contact with solution. An overview is presented of the standard transmission line model with two transport channels and a crosswise element. The simplest configurations are discussed: a single resistance in one of the channels, and either an interfacial capacitor or a RC transfer circuit at the pore's wall. The resulting relaxation functions are classified in terms of two characteristic frequencies: one for coupled transport and interfacial polarization and another one for the interfacial reaction. Subsequently, these models are extended in order to describe porous electrodes where the interfacial polarization displays complex properties, i.e., frequency dispersion. The capacitive element is described by a constant-phase element (CPE), and it is shown that the fractionary exponent provides an additional and measurable degree of freedom in the parameter space of the relaxation function, whose determination can be exploited as a supplementary tool for analysis. The analysis of impedance measurements of TiO_2 nanoporous photoelectrodes in negative bias voltage shows that the suggested approach is capable of identifying two characteristic relaxation frequencies in a frequency-resolved measurement on this system.

1. Introduction

Several types of porous or mixed-phase film electrodes such as nanostructured semiconductors and electroactive polymers have been extensively studied in recent years. Much of this work is focused on the use of the materials in technical applications including catalysis, electronics, photoelectronics, and solar energy storage and production. Porous electrodes operate in contact with an electrolyte by simultaneous transport of electronic and ionic species in the solid and liquid phase, respectively. Owing to the small scale of the constituents of the porous network, charge carriers in transit are always close to the surface, implying that transport and heterogeneous transfer processes are strongly coupled in these systems. Small signal frequency-resolved techniques appear as a major tool for resolving the mechanisms of carrier transport, trapping, and reaction. In these techniques, a particular steady state in given conditions of applied voltage, illumination, etc., is probed by means of a sinusoidal signal of small amplitude which barely disturbs the characteristics of the steady state. Furthermore, the response due to different processes is recorded in a single frequency sweep, according to the various characteristic frequency/times existing in the system. Ac impedance and other frequency-resolved techniques have been already applied to porous semiconductor electrodes of the materials TiO_2,[1−8] GaP,[9] and silicon.[10−12]

Advanced models are required for the impedance measurements of porous electrodes to be properly described and understood, due to the complexity of both the structure and the processes involved. In this paper we aim at providing new methods for analysis of porous film electrodes by electrochemical impedance. The work is focused in particular on the properties of porous nanocrystalline TiO_2 electrodes, which raise a growing interest in relation with their application to dye-sensitized solar cells[13] and electrochromic devices.[14]

In order to put the matter in a general perspective, a comparison follows of the features expected in a homogeneous electrode with those of a porous electrode in which two phases, liquid and solid, become mixed inside the electrode region. A homogeneous electrode with a macroscopically flat surface is shown schematically in Figure 1a. The equivalent circuit modeling the cell impedance is a series connection of elements, describing the division of the applied small-signal ac voltage in three parts: one at the bulk of the layer, another at the solid/liquid interface, and finally another one including the potential drop at bulk electrolyte and metal contacts. As is well-known from studies of the interfacial impedance Z_{if} of planar semiconductor electrodes,[15] several effects occur at the semiconductor/liquid contact including the capacitance and resistance of the space-charge region, the effect of surface states, the capacity and charge transfer resistance across the Helmholtz layer, and the diffusion of reacting species. Therefore, the form of Z_{if} may become quite complex, but nonetheless the various processes involved in Z_{if} are "localized" in the sense that the potential difference driving these processes obeys two conditions: it resides essentially at the semiconductor/electrolyte interface, and it is essentially independent of position on the surface. Or, to put it another way, the flux of carriers is always normal to the plane of the surface, and the current density is the same at any point in the surface. Consequently, Z_{if} can be described by the series and/or parallel combinations of resistive and capacitive components.

* Corresponding author. E-mail: bisquert@uji.es.
† Universitat Jaume I de Castelló.
‡ Hahn-Meitner Institut.
§ Universidade Federal de São Carlos.

10.1021/jp993148h CCC: $19.00
Published on Web 02/18/2000

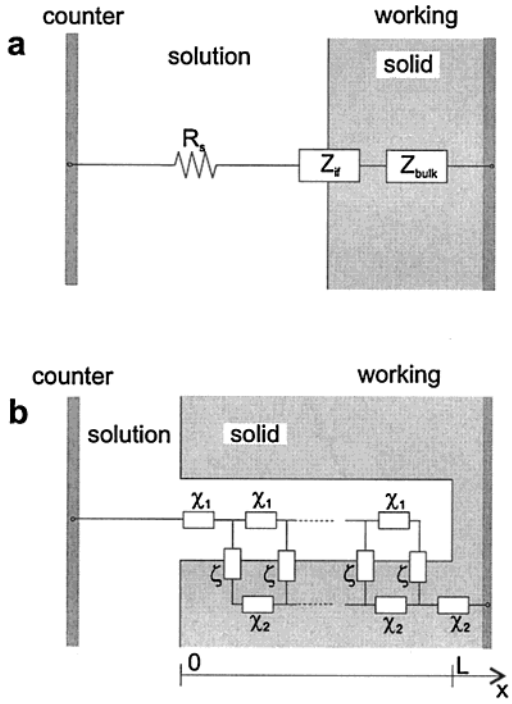

Figure 1. (a) Scheme of a compact electrode with a macroscopically flat surface. (b) Scheme of a porous electrode. The equivalent circuit models are explained in the text.

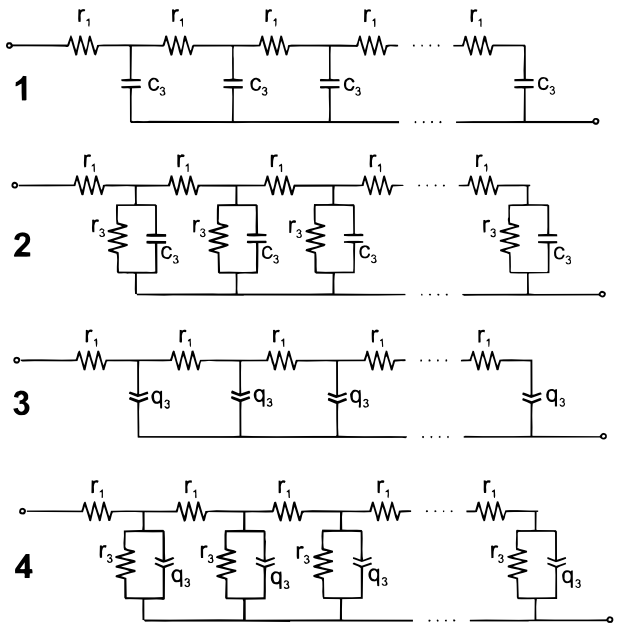

Figure 2. Transmission line representation of the models (1−4) for the impedance of porous electrodes discussed in the text.

In Figure 1b, a schematic illustration is provided of those cases where the two phases are closely mixed in space, i.e., because the layer is porous at a small scale. Both media are considered as effectively homogeneous and continuously connected phases. A standard equivalent circuit model is represented in Figure 1b that describes the essential features of electrical transport along each phase and the exchange of charge through the inner surface.[16] This model assumes that the dominant contribution to the current is electrical field driven rather than diffusive. Now the porous structure gives rise to the spread of electrical current in various directions. First, electrical charge can flow along each medium; the resulting ac currents are termed here $\tilde{\imath}_1$ and $\tilde{\imath}_2$ (the subscripts 1 and 2 denote the liquid and solid phase, respectively) and they follow the *x* direction in the scheme of Figure 1b, i.e., both $\tilde{\imath}_1$ and $\tilde{\imath}_2$ are *parallel* to the inner surface shown in the figure (see Figure 3). Moreover, current can flow in the direction *normal* to the inner surface due to electrochemical reactions and/or capacitive charging. Therefore, at a given location, $\tilde{\imath}_1$ may decrease (increase) with a corresponding increase (decrease) of $\tilde{\imath}_2$, the constraint being obeyed that $\tilde{\imath}_T = \tilde{\imath}_1 + \tilde{\imath}_2$ (the total current flowing through the external circuit) is independent of position. In accord with that description of electrical current distribution, the equivalent circuit branches at each point in each medium into an element that continues in the same medium, χ_1 or χ_2, and another element ζ that crosses the interface. The elements χ_1 and χ_2 describe a local ohmic drop at each point of the transport channels, depending on media conductivity and more generally on transport properties, whereas the element ζ describes an exchange of electrical charge at the interface owing to faradaic currents and polarization at the pore surface. (Obviously, the interfacial impedance ζ itself might consist on a complex equivalent circuit as formerly commented in relation with Z_{if}.) The branching in the equivalent circuit model is intended to occur in a continuous fashion, as described by the differential equations presented in section 2. The quantities χ_1 and χ_2 are impedances per unit length ($\Omega \cdot m^{-1}$) corresponding to the whole electrode area *A*, and ζ is an impedance length ($\Omega \cdot m$). The overall impedance is isomorphous to that of a transmission line. Regarding the electrical potential distribution, the simple assumption is made that an ac potential can be defined in each phase $\tilde{\phi}_1$ and $\tilde{\phi}_2$ which is, at each frequency, a unique function of position *x*; no radial distribution of potential into the pores or solid particles is considered. It follows that the ac potential difference between the two phases at a point *x*, i.e., the overvoltage in interfacial reactions, is $\tilde{\phi}_2 - \tilde{\phi}_1$.

As a simplest example we anticipate the presentation of a polarizable porous electrode to be more fully discussed in section 2. Assuming that the solid phase is highly conducting (i.e., a porous metal), then no hindrance to transport is to be expected in that phase and thus $\chi_2 \approx 0$. Clearly, phase 2 is an equipotential under that assumption, and the transmission line is accordingly short circuited at all points in phase 2. On the other hand, the flooded pore exhibits a distributed resistance ($\chi_1 = r_1$) which depends on the conductivity of the electrolyte. Electrical charge may be stored in the double layer at the pore's wall; this is represented by a capacitance per unit length c_3 in the exchange element ζ. In this manner, the general transmission line shown in Figure 1b gives rise to the first of the four models shown in Figure 2.

It must be emphasized that there are different types of assumptions regarding geometry and microstructure that lead to the transmission line model shown in Figure 1b.[17] One arrives at this picture either from the simple model of perfect cylinder geometry depicted in Figure 1b,[16] provided the pore is long compared with its diameter (for short pores one speaks instead of interfacial *roughness*), or from an effective macrohomogeneous description of two closely mixed phases,[18] e.g., a matrix of electrically connected semiconducting particles, or a permeable membrane. This second view is the most appropriate in the majority of applications.

The impedance of porous electrodes has been broadly discussed in the literature. Theoretical formulations have been developed and reviewed,[16−20] and applications have been presented to such systems as porous metal electrodes,[21−23] porous mixed-oxide electrodes,[24] ion exchange membranes,[25,26] and electroactive polymer-coated electrodes.[27−30] Transmission

line models appear also in connection with the ac response of a homogeneous layer with two oppositely charged carriers; a description of the ac electrical field inside the layer can be obtained from Poisson's equation[31] and also from the electroneutrality condition.[32,33] An account of static disorder in porous electrodes was attempted by means of random network models.[34]

We elaborate here on the theory of porous electrodes mainly in two directions. A first aspect to be noticed, in relation with the new technologies cited above, is the fact that a restricted margin of variation of the steady-state voltage may switch the solid phase from a significant electronic conductivity to an insulating configuration. Consequently, the relaxation function adopts several distinct shapes or forms, depending on the values of such parameters as bulk conductivity or electrode thickness. Therefore, a first point to be addressed is the complete characterization of the relaxation functions, as a function of relevant parameters. The properties of the simplest relaxation functions are presented below. A classification scheme is derived on the basis of the various characteristic frequencies present in a given model.

Another major aspect that must be considered is the complexity of the medium at the microstructural level. One frequently encounters, as a consequence, such features as anomalous diffusion and capacitive dispersion in the impedance response, which are quite difficult to treat in the framework of the conventional idealized models. In this connection, our second point of concern is to provide generalized models to account for the complexity in the medium. Here we shall be focusing our attention on the effect of the interfacial impedance ζ. The main emphasis is laid on the role of the fractionary exponents that are customarily used to describe the effect of static or dynamic disorder in the system. Also briefly commented is the description of memory effects and dispersive transport through the transport impedances χ_1 and χ_2.[35]

While the general double-channel transmission line represented in Figure 1b involves a wide variety of possible models, it must nevertheless be noticed that such models refer to "volume" processes which are distributed over the entire electrode region. In addition, one must take account of possible processes related to injection and/or blocking of charge carriers at the macroscopic boundaries. Injection is commonly treated as an electrochemical reaction at the contact, giving rise to a Randles circuit connected at the end points of the line.[31,36,37] On the other hand, the effect of blocking at the boundary of transport channels can be modeled by suitable boundary conditions in the solution of the differential equations determining the impedance.[38,39] The distinction between the manifestation of volume and boundary processes in the impedance of thin electrodes was recently discussed.[40]

It must be noticed at the outset that transport and reaction properties of porous electrodes depend on the structure and chemical constituents of the phases and on the mechanisms involved. Here we try to omit the details of the structure and mechanisms as much as possible and to extract simple and quite general features which will remain true for a large class of systems. An analysis of impedance measurements on TiO_2 nanostructured photoelectrodes presented below shows that the generalized models provide an accurate quantitative description of complex porous electrodes.

2. Models

2.1. Impedance of the Two-Channel Transmission Line. A brief outline is presented of the calculation of the impedance of a porous electrode. As stated before, $\tilde{\phi}_k$ and $\tilde{\imath}_k$ denote the ac

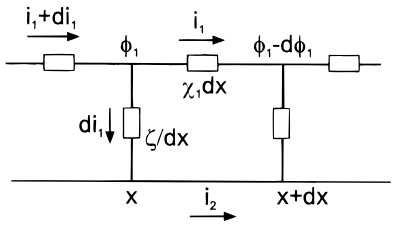

Figure 3. Local variation of ac electrical potential and conduction current in a transmission line. Channel 2 is short-circuited ($\chi_2 = 0$).

parts of the applied voltage, and of the total electric current, respectively, in the two phases ($k = 1, 2$). χ_1 and χ_2 carry the information about the transport of the respective carrier in each phase (and in particular the possible frequency dependence of the conductivity[35]). We first consider the case when the solid phase possesses a large conductivity ($\chi_1 \gg \chi_2$). Then the solid phase is an equipotential ($\chi_2 = 0$) which is taken as the voltage reference so that $\tilde{\phi}_2 = 0$. This restriction applies to many situations of practical interest, and the mirror case where the solid phase is the more resistive ($\chi_1 \ll \chi_2$) is obtained by interchanging subscripts 1 and 2.

A major assumption adopted (as in the classical theory of porous electrodes[16,18]) is that transport in the more resistive phase is driven by the gradient of the electrical potential $\tilde{\phi}_1$. From Figure 3, the following equation is easily deduced

$$\frac{\partial \tilde{\phi}_1}{\partial x} = -\chi_1 \tilde{\imath}_1 \tag{1}$$

which is simply the statement of Ohm's law in channel 1. As discussed in more detail elsewhere[35] this corresponds to select the drift term in the electrochemical potential; further remarks about this point are presented below in the Discussion section. On the other hand, ζ determines the electrical current flow at the flooded pore wall which is driven by the potential difference between the two phases, $\tilde{\phi}_2 - \tilde{\phi}_1$. Since the solid phase is short-circuited ($\tilde{\phi}_2 = 0$), from Figure 3 it follows now that

$$\frac{\partial \tilde{\imath}_1}{\partial x} = -\frac{1}{\zeta}\tilde{\phi}_1 \tag{2}$$

We shall assume that quantities χ_1, χ_2, and ζ are position-independent, meaning that these quantities are unique functions of frequency. This restriction provides a considerable simplification of analysis.

The ionic current vanishes at the end of the liquid channel

$$\tilde{\imath}_1(L) = 0 \tag{3}$$

and the total electrode impedance is given by

$$Z = \frac{\tilde{\phi}_1(0)}{\tilde{\imath}_1(0)} \tag{4}$$

The solution of eqs 1−4 is

$$Z = (\zeta\chi_1)^{1/2} \coth(L/\lambda) \tag{5}$$

where L is the thickness of the porous layer and λ is a penetration length

$$\lambda = (\zeta/\chi_1)^{1/2} \tag{6}$$

The approximation of a perfect conductor in one of the channels of the transmission line does not apply in some

situations, especially when the relative conductivities in the ionic and electronic media achieve comparable magnitudes. Then one must resort to the solution of the transmission line model for arbitrary values of χ_1 and χ_2,[35] generalizing eq 5:

$$Z = \frac{\chi_1\chi_2}{\chi_1+\chi_2}\left(L + \frac{2\lambda}{\mathrm{sh}(L/\lambda)}\right) + \lambda\frac{\chi_1^{\,2}+\chi_2^{\,2}}{\chi_1+\chi_2}\coth(L/\lambda) \quad (7)$$

where $\lambda = [\zeta/(\chi_1 + \chi_2)]^{1/2}$.

The expressions of χ_1, χ_2, and ζ must be specified for eqs 5 and 7 to be used in the analysis of the impedance measurements. To this end, one can proceed basically in two ways. Kinetic models may be postulated that lead to eqs 1 and 2. This provides a physicochemical foundation to the forces and hindrances involved in the system's response. In the absence of sufficient information about the system's fundamentals, one may attempt to describe χ_1, χ_2, and ζ by suitable equivalent circuits in order to match the observed spectra. By this means valuable knowledge about the system's behavior may be acquired, by varying the control parameters of the experiment.

Since the aim in this paper is to establish quite general models, independent of system specifics, some reasonable and generally valid assumptions shall be adopted about the basic elements in the transmission line.

2.2. Simplest Models for the Impedance of Porous Electrodes. It will be assumed hereafter that $\chi_2 = 0$ and that the more resistive channel is modeled by a distributed resistance

$$\chi_1 = r_1 \quad (8)$$

and thus the total resistance (Ω) distributed in the resistive channel is given by

$$R_1 = Lr_1 \quad (9)$$

The choice of interfacial properties (ζ) gives rise to different models. Here an overview of the simplest and most widely used models for the impedance of porous or mixed-phase electrodes is presented, emphasizing the classification of different patterns of response. The equivalent circuits representing the various models discussed in this section are shown in Figure 2.

Model 1. An ideally polarizable distributed interface is described by a capacitance c_3 which is commonly attributed to double-layer effects.

$$\zeta = \frac{1}{ic_3\omega} \quad (10)$$

The total capacitance (F) in the walls of the pores is

$$C_3 = Lc_3 \quad (11)$$

The only characteristic frequency in this model is given in the following expression.

$$\omega_L = \frac{1}{R_1C_3} = \frac{1}{L^2r_1c_3} \quad (12)$$

The impedance may be written in the form

$$Z = R_1(i\omega/\omega_L)^{-1/2}\coth[(i\omega/\omega_L)^{1/2}] \quad (13)$$

The frequency ω_L separates quite different domains of behavior, as seen in Figure 4a. In the high-frequency branch ($\omega > \omega_L$) one obtains

$$Z = \left(\frac{R_1}{C_3}\right)^{1/2}(i\omega)^{-1/2} \quad (14)$$

Equation 14 is often termed a "Warburg" impedance, appearing as a slope 1 line in the complex impedance plot. The same type of behavior arises from diffusion in a semiinfinite medium, although no diffusion in the sense of Fick's law is involved in the interpretation given here (this point is commented in the Discussion section).

At low frequencies ($\omega < \omega_L$), eq 13 is simplified to the series combination of two elements: a resistance and the whole capacitance at the pore's surface, as indicated in eq 15.

$$Z = \frac{1}{3}R_1 + \frac{1}{iC_3\omega} \quad (15)$$

The two domains of frequency behavior which have been found may alternatively be distinguished in terms of the penetration length

$$\lambda = \frac{L}{(i\omega/\omega_L)^{1/2}} \quad (16)$$

The Warburg response obtains if the penetration length is shorter than the pore's length ($\lambda < L$); otherwise ($\lambda > L$) the capacitive behavior prevails. Therefore, it can be said that the frequency ω_L is related to the finiteness of size of the electrode.

Model 2. A second widely used model describes an interfacial reaction by inclusion of a charge transfer resistance in parallel to the capacitance in ζ (see Figure 2).

$$\zeta = \frac{r_3}{1 + ir_3c_3\omega} \quad (17)$$

The total wall resistance is

$$R_3 = \frac{r_3}{L} \quad (18)$$

The system has now two characteristic frequencies, ω_L in eq 12, and the frequency ω_3 of the transfer process, with the value

$$\omega_3 = \frac{1}{R_3C_3} = \frac{1}{r_3c_3} \quad (19)$$

The impedance adopts the form

$$Z = \left(\frac{R_1R_3}{1 + i\omega/\omega_3}\right)^{1/2}\coth[(\omega_3/\omega_L)^{1/2}(1 + i\omega/\omega_3)^{1/2}] \quad (20)$$

Looking now at the dc resistance resulting from eq 20, one finds

$$Z_{dc} = (R_1R_3)^{1/2}\coth[(R_1/R_3)^{1/2}] \quad (21)$$

Interestingly, two distinct limiting cases appear according to the relative magnitude of the total resistances:

$$Z_{dc} = \frac{1}{3}R_1 + R_3 \qquad (R_3 > R_1) \quad (22)$$

$$Z_{dc} = (R_1R_3)^{1/2} \qquad (R_1 > R_3) \quad (23)$$

The following relationship shows that these two cases are determined by the relative position of the characteristic

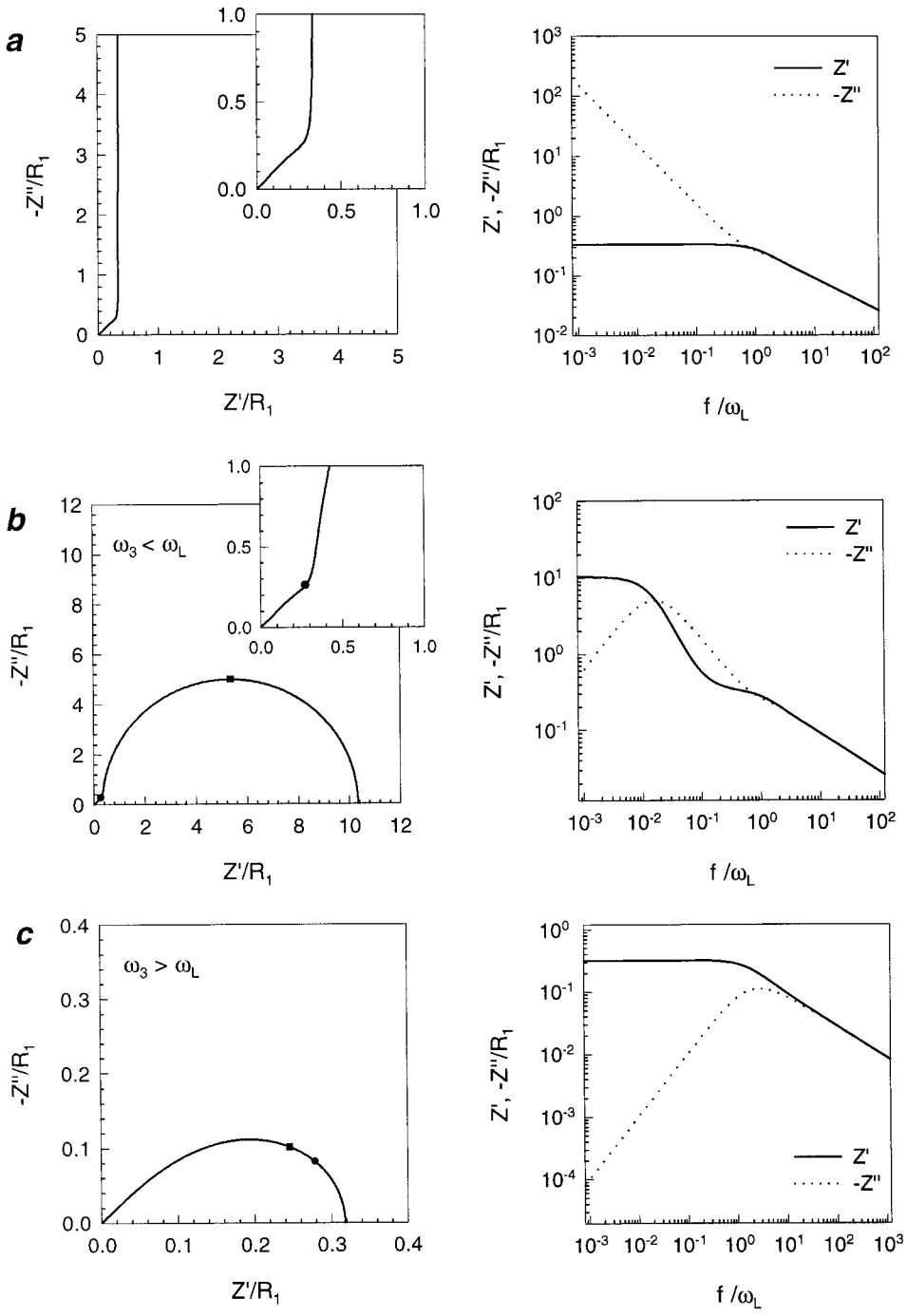

Figure 4. Impedance ($Z = Z' + iZ''$) of the transmission line models possessing a capacitance in the interfacial impedance ζ. Complex plane representation (left panels) and Bode plot representation (right panels). (a) Model 1, eq 13. (b, c) Model 2, eq 20. The marked points correspond to frequencies $f = \omega_L$ (●) and $f = \omega_3/2\pi$ (■).

relaxation frequencies in the frequency axis:

$$\frac{\omega_3}{\omega_L} = \frac{R_1}{R_3} \tag{24}$$

The relaxation function adopts quite different shapes in the two situations, as shown in Figure 4b,c.

First, for $\omega_L > \omega_3$ one finds the following trends. At frequencies $\omega > \omega_3$ one gets model 1, i.e., the Warburg line with slope 1 at high frequencies with an elbow near ω_L. At low frequency, eq 25 is a good approximation to eq 20. Therefore, in the present model as the frequency decreases the charge transfer resistance gives rise to a semicircle at low frequency, as seen in Figure 4b.

$$Z = \frac{R_3}{1 + i\omega/\omega_3} \tag{25}$$

From this result it can be concluded that at low frequency "the impedance of a cylindrical pore is equal to that of the flat electrode of same area as the developed surface," as stated by Candy et al.[21]

However, the other case ($\omega_3 > \omega_L$) provides another type of behavior. Now, at all frequencies one has within good approximation

$$Z = \left(\frac{R_1 R_3}{1 + i\omega/\omega_3}\right)^{1/2} \tag{26}$$

Equation 26 gives rise again to Warburg behavior at high frequency ($\omega > \omega_3$), but no upturn appears now in the complex impedance plot (Figure 4c). At low frequency ($\omega < \omega_3$), the plot closes to a semicircle corresponding to parallel connection of the dc resistance (eq 23) and the capacitance C_{lf}.

$$C_{lf} = \frac{1}{2}\left(\frac{R_3}{R_1}\right)^{1/2} C_3 \tag{27}$$

2.3. Impedance of Complex Transport and Polarization Processes. The simple models overviewed in the preceding paragraphs are unsuited to accurately describe many of the porous thin film electrodes that are practically found in recent technologies and applications. One encounters most frequently systematic deviations from the basic models, giving rise to severe problems of model validity assessment and parameter determination.

In our view, these deviations are explained in many cases by the excessively idealized nature of the elements postulated in the ordinary distributed circuits. While the basic transmission line models discussed above incorporate the *structural* aspects of voltage and current distribution (i.e., the mixture of phases, and the fact that the macroscopic boundaries are impermeable to different species), one must furthermore deal with the considerable degree of inhomogeneity, complexity, and disorder usually present in the electrodes. This second aspect has been generally disregarded in the literature. Therefore, one is naturally led to postulate more realistic elements in the transmission line. We consider in turn the transport elements χ_i and the interfacial impedance ζ.

(*a*) *Anomalous Transport Effects.* It is often assumed, in discussing the impedance of porous electrodes, that a distributed resistance (r_1 or r_2 in our notation) sufficiently describes the transport events. A constant resistance is evidently linked to a frequency-independent conductivity. Thus, the electronic resistivity can be expressed as

$$r_2 = \frac{1}{A\sigma_e} \tag{28}$$

in terms of the dc conductivity

$$\sigma_e = \frac{q^2 \bar{n}}{k_B T} D_e \tag{29}$$

where D_e is the diffusion coefficient for the electrons, q is the elementary charge, and $\bar{n}$ stands for the dc concentration of free electrons (the decrease of effective volume due to porosity is neglected). However, when electronic carriers diffuse or drift in an amorphous semiconductor, or in a material containing many traps, the number of electrons effectively contributing to the flux depends on the frequency of the sinusoidal signal.[41] The ac conductivity acquires a frequency dependence, which can be expressed, for many systems, according to the following law:[42]

$$\sigma(\omega) = \sigma(0)[1 + (i\omega/\omega_m)^p] \tag{30}$$

Therefore, two different regimes of behavior exist depending on the value of the modulation frequency: a dc or quasi-dc conductivity $\sigma(0)$ at low frequencies crossing over to an apparent power law at high frequencies; ω_m is the crossover frequency, and the fractionary exponent obeys $0 < p < 1$. For a system with electronic or ionic carriers displaying anomalous transport, a model for the porous electrode can be constructed by inclusion of eq 30 in the respective resistivity of the phases (eq 28). The anomalous transport should exert a notorious influence on the overall impedance response once the power law behavior is onset above ω_m; for instance the high-frequency "Warburg" part of the spectra may become markedly curved in the complex plane representation. The impedance of porous electrodes that exhibit anomalous transport has been thoroughly discussed in another paper.[35]

(*b*) *Capacitive Dispersion at the Interface.* In the region of transition between two phases, a potential difference exists which is sustained by charge stored at the interface. The differential relationship between the charge at the boundary and the electrical potential is the interfacial capacitance. The capacitance is often a function of the electrical potential; a detailed model can be established if the spatial distribution of electrical charge as a function of potential is known, as in the Mott−Schottky model for space-charge polarization at the semiconductor−liquid junction. In addition, the capacitance of a polarizable interface may become, at each value of voltage, a function of *frequency*, a fact which is sometimes dubbed capacitive dispersion.[43] Experimentally, this is the rule rather than the exception, and the impedance of different types of interfaces is found to behave as a constant phase element (CPE):[43−45]

$$Z = \frac{1}{Q}(i\omega)^{-\beta} \tag{31}$$

The impedance of eq 31 consists on a tilted straight line in the complex plot. The exponent β can be any number in the range $0 < \beta < 1$, and Q is a constant with dimension F s^{n-1}. The value $\beta = 1$ recovers a perfect capacitor but, as already emphasized, it is found experimentally that $\beta < 1$. In contrast with the voltage dependence of the interfacial capacitance, it proves extremely difficult to justify the observed frequency dependence on a theoretical basis. One suspects that some basic and universal relaxation phenomena must be involved in CPE behavior, because it appears in quite different systems, but it has not yet been established what the mechanism is. It is nonetheless known that CPE behavior consists on intrinsic electrode polarization effects unrelated to faradaic currents crossing the interface.[44] Notice that eq 31 is compatible with the definition of an ideally polarizable interface, since $|Z| \to \infty$ when $\omega \to 0$.[45] It was pointed out that, although eq 31 contains a dissipative component at finite frequencies, various effects not involving heterogeneous transfer can be responsible for the dissipation of energy.[45] The polarization capacitance of the semiconductor/solution interface has been often reported to exhibit frequency dispersion of CPE type.[46,47] It was asserted that the dispersion depends on the microroughness of the electrode surface and on the conductivity of the electrolyte solution.[48]

2.4. Models for the Impedance of Porous Electrodes Exhibiting Complex Interfacial Processes. In this section, models for the porous electrode are developed in which the inner surface exhibits a frequency-dependent capacitance.

Model 3. The situation is considered again as in model 1 where a negligible level of charge transfer occurs across the distributed interface. The blocking interface is now described by a dispersive capacitance as given by a CPE (see Figure 2). Therefore, this model is defined by

$$\zeta = \frac{1}{q_3}(i\omega)^{-\beta} \tag{32}$$

where q_3 is a constant, and $0 < \beta < 1$. The assumption in eq 32 is justified on the grounds that the inner surface in a realistic mixed-phase electrode should display the characteristic transfer function observed in most planar electrodes.

From the above assumptions one gets

$$\lambda = (r_1 q_3)^{-1/2}(i\omega)^{\beta/2} \tag{33}$$

and therefore

$$Z = \left(\frac{r_1}{q_3}\right)^{1/2}(i\omega)^{-\beta/2}\coth[L(r_1 q_3)^{1/2}(i\omega)^{\beta/2}] \tag{34}$$

The characteristic frequency of finite-size effect must now be defined as

$$\omega_L = \frac{1}{(r_1 q_3 L^2)^{1/\beta}} = \frac{1}{(R_1 Q_3)^{1/\beta}} \tag{35}$$

where $Q_3 = Lq_3$ (with dimension F $s^{\beta-1}$). The electrode impedance may also be expressed in a more compact form as

$$Z = R_1(i\omega/\omega_L)^{-\beta/2}\coth[(i\omega/\omega_L)^{\beta/2}] \tag{36}$$

The complex plane plot exhibits an elbow around ω_L that separates two domains of behavior, as illustrated in Figure 5a. Capacitive dispersion occurs at low frequencies ($\omega < \omega_L$); i.e., eq 36 adopts the form in eq 37, consisting on a CPE with exponent β, in series with a resistance.

$$Z = \frac{1}{3}R_1 + \frac{1}{Q_3}(i\omega)^{-\beta} \tag{37}$$

On the other hand, at high frequencies ($\omega > \omega_L$) the impedance deviates from the exact slope 1 behavior found in the previous models. Instead, one finds

$$Z = \left(\frac{R_1}{Q_3}\right)^{1/2}(i\omega)^{-\beta/2} \tag{38}$$

A major feature of this model is that the fractionary exponent at low frequency exactly *doubles* that at high frequency (see Figure 5a), because the dispersive feature in both regimes of frequency stems from element q_3. The doubling of exponents can be checked in practice by piecemeal fit of the two regimes identified in eqs 37 and 38. This provides a quite stringent criterion to decide whether the impedance spectra are actually described by the model.

Model 4. The effect of an interfacial reaction in the pore surface can be modeled by adding a parallel charge transfer resistance to the interfacial impedance of Model 3 (see Figure 2). Then one has

$$\zeta = \frac{r_3}{1 + r_3 q_3(i\omega)^{\beta}} \tag{39}$$

Equation 39 describes a generalized transfer process introduced by Le Mehaute et al.[49,50] in relation with transfer across a fractal interface. The trace of ζ in the complex impedance plot is a depressed and symmetric semicircle, which is also obtained from a Cole−Cole distribution in complex dielectric permittivity plots. It should be noted that an alternative description of the transfer process was proposed, giving rise instead to a distribution of the Cole−Davidson type.[51,52]

The characteristic frequency ω_3 of the interfacial process is given by

$$\omega_3 = \frac{1}{(r_3 q_3)^{1/\beta}} = \frac{1}{(R_3 Q_3)^{1/\beta}} \tag{40}$$

so that eq 39 may be also written as

$$\zeta = \frac{r_3}{1 + (i\omega/\omega_3)^{\beta}} \tag{41}$$

and the electrode impedance is

$$Z = \left[\frac{R_1 R_3}{1 + (i\omega/\omega_3)^{\beta}}\right]^{1/2}\coth((\omega_3/\omega_L)^{\beta/2}[1 + (i\omega/\omega_3)^{\beta}]^{1/2}) \tag{42}$$

An analysis of relaxation function 42 can be performed along the same steps previously followed in model 2. The value of the quotient

$$\frac{\omega_3}{\omega_L} = \left(\frac{R_1}{R_3}\right)^{1/\beta} \tag{43}$$

determines the shape of the impedance spectra. For $\omega_L > \omega_3$ (or $R_3 > R_1$), one obtains a line at high frequency (with less than 45° inclination, for $\beta < 1$) and a low-frequency arc, as shown in Figure 5b. The elbow is at frequency (Hz) $f = \omega_L$, and the apex of the arc is at $f = \omega_3/2\pi$. For $\omega \gg \omega_3$ the same behavior as in model 3 is found (eqs 37 and 38), while at low frequency the electrode impedance can be simplified to eq 44. The depressed arc at low frequencies is the manifestation of the interfacial impedance. The arc is displaced in the direction of the positive real axis, according to eq 44.

$$Z = \frac{R_3}{1 + (i\omega/\omega_3)^{\beta}} + \frac{1}{3}R_1 \tag{44}$$

The other case is for $\omega_3 > \omega_L$ (or $R_1 > R_3$), represented in Figure 5c. Then the impedance can be approximated at all frequencies by the function

$$Z = \left(\frac{R_1 R_3}{1 + (i\omega/\omega_3)^{\beta}}\right)^{1/2} \tag{45}$$

Here two domains of frequency are identified: eq 38 for $\omega > \omega_3$, or else a semicircle at low frequency corresponding to parallel connection of the dc resistance (eq 21) and a CPE with an impedance

$$Z_{\text{if}} = 2\left(\frac{R_1}{R_3}\right)^{1/2}\frac{1}{Q_3}(i\omega)^{-\beta} \tag{46}$$

The doubling of exponents also exists in model 4 and can be confirmed by separate fits of an arc to the low-frequency data, and a CPE to the high-frequency part of the spectra.

3. Experimental Section

TiO_2 nanoparticles and electrodes were prepared by a method similar to that followed by Barbé et al.[53] The substrate used for the TiO_2 thin-layer electrodes was a glass covered with conductive fluorine-doped tin oxide (FTO, Nippon Sheet Glass,

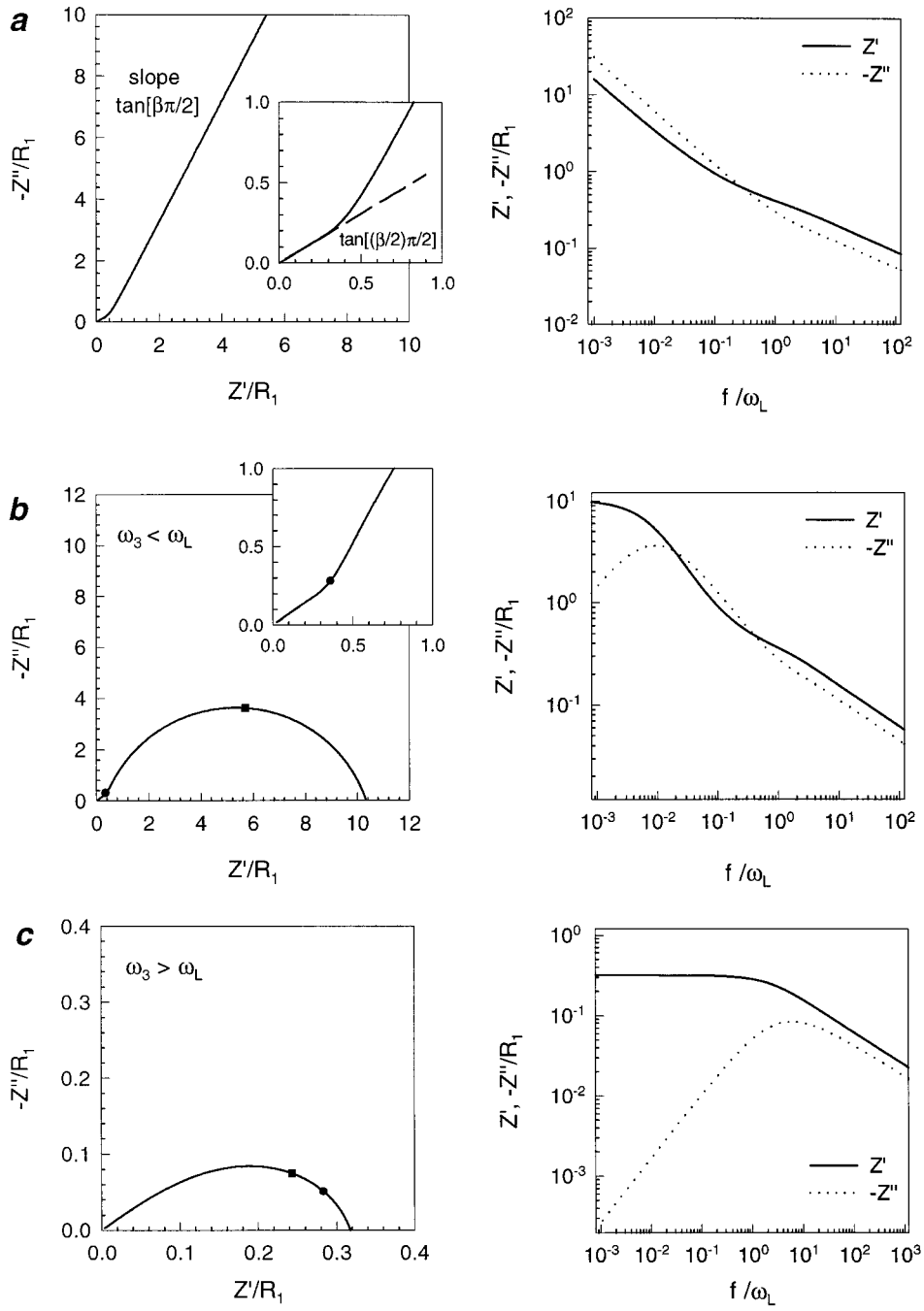

Figure 5. Impedance ($Z = Z' + iZ''$) of the transmission line models possessing a constant phase element in the interfacial impedance ζ. Complex plane representation (left panels) and Bode plot representation (right panels). (a) Model 3, eq 36. (b, c) Model 4, eq 42. The marked points correspond to frequencies $f = \omega_L$ (●) and $f = \omega_3/2\pi$ (■).

Hyogo, Japan). Two series were done, resulting in TiO_2 (pure anatase) layers of thickness of about 7.0 μm for the sample labeled Tk3a, and 8.6 μm for that called Tk6a. The particle size was about 10 nm in both cases. Samples were introduced in a three-electrode electrochemical cell containing distilled water adjusted at pH 2 with pure sulfuric acid. Counter electrode was Pt and reference electrode was a standard Ag/AgCl (in KCl 3 M solution) to which the quoted dc voltages are referred.

Impedance measurements were done with an Autolab impedance analyzer connected to a PC which acquires the data and controls the equipment. Illumination of the samples was done with a 150 W mercury lamp filtered to suppress wavelengths shorter than 340 nm. Light intensity was controlled by a calibrated diaphragm. A mobile lens was used to ensure uniformity of the illuminated area.

In all cases the series resistance (as determined by the intercept at high frequency) was subtracted in the reported spectra, to better display the agreement with the simulations presented in section 2.

4. Results

Figure 6 illustrates measurements of impedance in the dark and at illumination in sample Tk6a under a negative bias of 0.20 V. In this configuration strong accumulation occurs in the array of TiO_2 particles. Electrons are injected to the solution, giving rise to hydrogen evolution. The spectra are very well

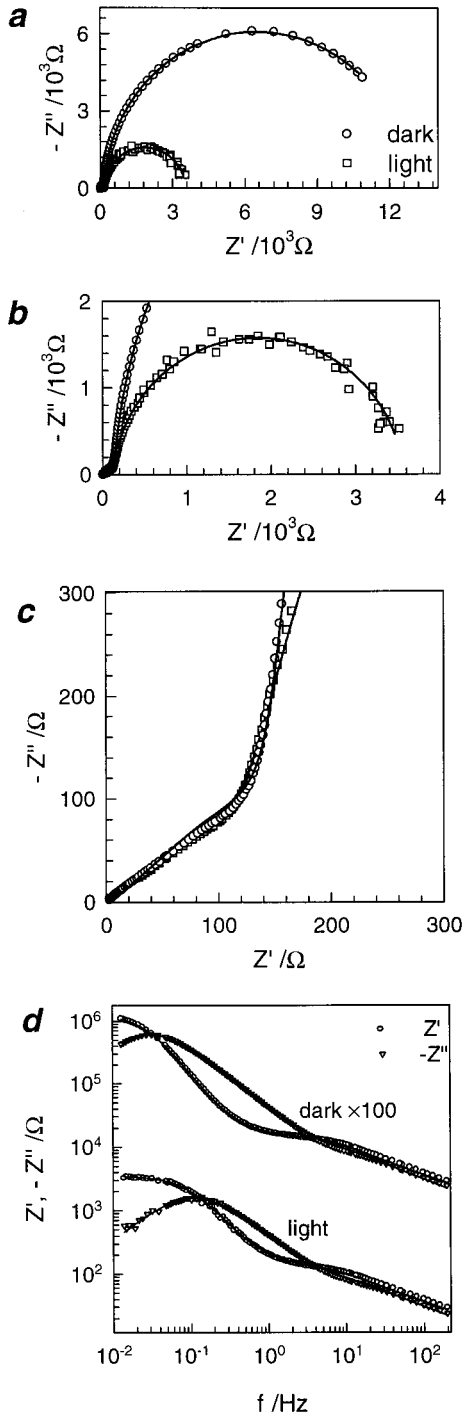

Figure 6. Impedance response of a TiO_2 nanoporous electrode (sample Tk6a) in acidic water (pH 2), at −0.20 V bias vs Ag/AgCl, in the dark and at supra-band gap illumination. The lines are fits of eq 42 to the data. (a−c) Complex plane plots. (d) Bode plot representation (data in the dark are offset for clarity of display).

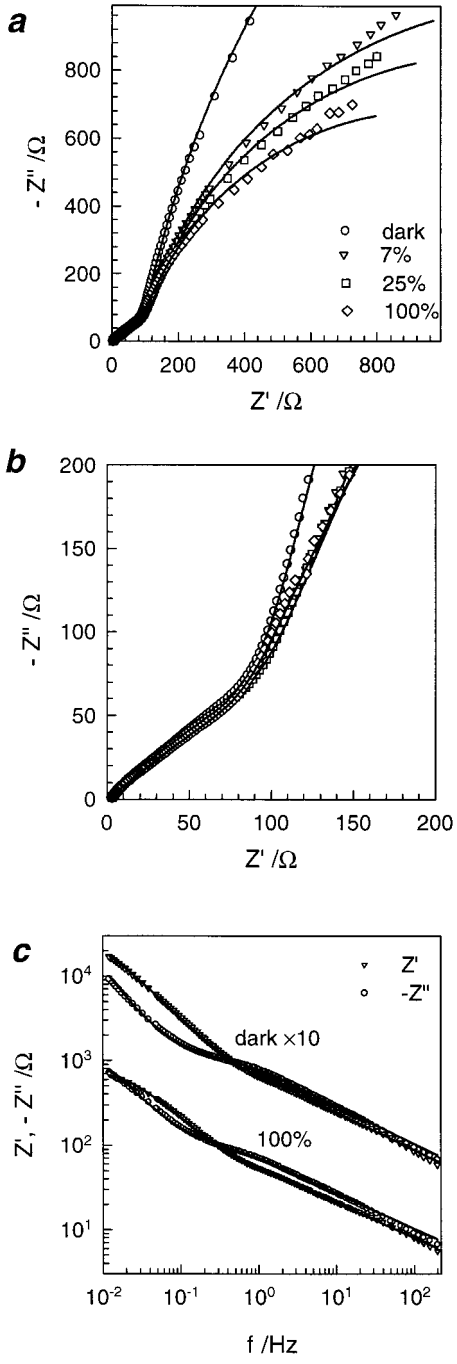

Figure 7. Impedance response of a TiO_2 nanoporous electrode (sample Tk3a) in acidic water (pH 2), at −0.25 V bias vs Ag/AgCl, in the dark and at supra-band gap illumination at various light intensities. The lines are fits of eq 42 to the data. (a, b) Complex plane plots. (c) Bode plot representation (data in the dark are offset for clarity of display).

resolved, exhibiting a remarkable agreement with model 4. Fits of impedance function in eq 42 (continuous line in Figure 6) provide excellent results, and therefore one is able to determine the value of two characteristic relaxation frequencies: ω_L and ω_3. It is assumed that the electrolyte resistance can be neglected ($r_1 \approx 0$), as justified below. Notice that eq 34 adopts then the form $\omega_L{}^{-\beta} = r_2 q_3 L^2$. From the fit results it is found that neither r_2 nor q_3 is influenced by the incident light intensity, and therefore the relaxation frequency ω_L remains fixed as the light intensity varies, which can be readily appreciated in Figure 6c. On the other hand, r_2 exhibits an exponential dependence on the bias voltage. Values of the dispersive exponent are approximately equal to $\beta = 0.96$.

At high frequencies and more positive voltages than those reported here, the high-frequency "Warburg" part of the spectra developed a downward curvature which was ascribed to dispersive transport of electrons.[35]

Figure 7 shows measurements of impedance in sample Tk3a under a negative bias voltage of 0.25 V, in the dark and at illumination. The measured data were fitted to the relaxation function eq 42 of model 4, and values near $\beta = 0.86$ were obtained. The trends observed in these measurements are analogous to those of sample Tk6a. Notice in particular in Figure

7b that the elbow marking the characteristic frequency ω_L stays fixed independently of the applied light intensity.

5. Discussion

5.1. Models. The impedance of electrochemical cells containing homogeneous electrodes is usually analyzed in terms of a simplest geometry in which all boundaries lie in parallel planes. In porous electrodes the measured impedance is the cumulative signal of spatially distributed processes involving the variation with position throughout the porous layer of electrical currents and electrochemical potential.[54] To infer the basic distributed processes from the unique measured response is a primordial aim of analysis, enabling one to decouple transport and reaction processes and to identify and locate the physicochemical origin of the observed features of the response. Transmission line models serve this purpose in that the entire equivalent circuit is constructed according to the properties of the various phases and interfaces present in the electrode. The number and type of circuit elements that model basic processes in the transmission line determine a relaxation function, which may exhibit various patterns of response. These can be classified either according to the relative location of characteristic relaxation frequencies in the frequency axis, or in terms of total values of the distributed impedances (eq 24). The first method is better suited to identify the *form* of the relaxation function; while using the second method, the magnitudes such as R_1 and R_3 fix the absolute *scale* of different parts of the spectra in the complex impedance plane.

The various domains of frequency behavior existing in each case can be ascribed to the joint response of certain elements of the line. This observation acquires central importance when models with fractionary exponents enter the scheme. Then, the dispersive feature becomes apparent in distinct domains of frequency, pointing out to a common origin in terms of microscopical processes. What is clarified, quite unambiguously, is that the relaxation is composed of the coupling in a short spatial scale of transport *and* inner interfacial processes (although the detailed transport mechanism is more open to question, as discussed below). Therefore, while frequency dispersion is usually regarded as a nuisance, the view is adopted here that the fractionary exponents are measurable parameters which can be exploited as a supplementary tool for analysis.

Relaxation functions of the same type as those of the dispersive models presented in section 2 (models 3 and 4) have been considered in the literature, although reported applications of these models are scarce. In fact, recently reported measurements exhibiting frequency dispersion and following apparently the trends of model 3 were instead analyzed in those works[26,55] using model 1. Impedance functions resembling that of model 3 were suggested in relation with different types of nonuniform diffusion in finite layers.[56,57] This interpretation is different than that adopted here. On the other hand, model 4 (with a different notation) was presented by Gassa et al.[23] in direct relation with porous electrodes. The authors obtained excellent fits to measurements of impedance in porous Raney nickel and other types of electrodes. However, the authors did not explicitly mention the doubling exponent feature of the model.

An important aspect that must be considered in the interpretation of impedance measurements is the well-known problem of ambiguity of equivalent circuit models. It is worth emphasizing that different types of assumptions give rise to relaxation functions with close resemblance of those presented in this work. In the theory presented in section 2, only the *drift* term was maintained in the electrochemical potential as a simplifying assumption. If, alternatively, one selects the *diffusion* term, an impedance function can be obtained[39] which is mathematically *identical* to that of model 1, although in that case the diffusion overvoltage is at the macroscopic interface driving the supply of diffusing species at the outer edge of the porous layer. Furthermore, if a reaction term is included in the diffusion theory, then an impedance could be found which is mathematically equal to that of model 3. Drift and diffusion-based impedance models were compared in the paper by Gabrielli et al.[58] In these and other cases,[32] different physicochemical models give rise to the *same* equivalent circuit, apparently there being no fundamental reason for that. A similar equivalence occurs as one solves the equations in the time domain in order to discuss evidence from time-transient techniques. Impedance and time-transient techniques are in this respect underdetermined, even in the face of spectra with very detailed features, and a good fit to the relaxation function does not validate the physical assumptions in a model. In these situations, extensive experimental evidence is required in combination with knowledge of electrode properties and additional information by complementary techniques.

Of course, simplifying assumptions may be relaxed and models of more general validity can be envisaged, but the solution of the problem becomes rather involved. It will be recalled that some major assumptions have been adopted in this work in order to obtain analytically closed solutions: position-independent impedance elements were assumed, and the effect of steady-state currents and electrical potential was not considered. Some authors have analyzed by numerical means of solution the effect of inhomogeneity[59] and steady-state currents and electric fields.[60]

Finally, we may notice that dispersion of frequency in distributed equivalent circuits, the central motive of this paper, can be realized in diffusion impedances as well, on the basis of theories of anomalous diffusion.[61]

5.2. Impedance of TiO_2 Nanoporous Electrodes in Aqueous Electrolyte. As already emphasized, the impedance response in the considered domain of steady-state applied voltage is accurately described by model 4. The following meaning is attached to the elements in the distributed equivalent circuit: r_2 (resistivity in the semiconductor matrix), r_3 (charge transfer resistance at the TiO_2/solution interface), and q_3 (interfacial CPE). The reason to attribute the resistive transport channel to the solid phase is that the element r_2 was observed to depend exponentially on the value of the bias voltage. Therefore, assuming a constant diffusion coefficient for the electrons D_e (eq 29), the observed variation of r_2 with steady-state voltage is interpreted in terms of a displacement of the Fermi level, determining the dc concentration of free electrons $\bar{n}$.

As regards the influence of illumination, it was already stressed above that r_2 remains almost constant as the light intensity varies at a given value of bias voltage. Therefore, according to eqs 28 and 29 the effect of photogenerated carriers is unnoticeable in the electronic conductivity, which is determined by the background of substrate-supplied electrons.

On the other hand, photogeneration promotes a modification of the charge transfer resistance r_3, as implied by the change of size of the low-frequency arcs in Figures 6a and 7a (the total span of the arc along the real axis gives R_3). Understanding the significance of the variation of the ζ-elements (r_3 and q_3) is complicated by the fact that H^+ is known to enter the TiO_2 matrix under cathodic bias.[62,63] Nonetheless, since the capacitive element q_3 maintains an almost stationary value in the various runs, it appears that the modification of r_3 must be ascribed to the influence of light.

Our experimental results for the impedance of TiO_2 nanoporous electrodes have illustrated the capabilities of the doubling-exponent models. Since the interfacial impedance and the transport elements have been identified and decoupled, it should be possible to proceed to suitable interpretations of interfacial properties according to the known electrochemical properties of semiconductor surfaces. Another interesting subject is whether the electronic carriers are displaced by migration or diffusion[2,64] and, closely related, what is the distribution of electrical potential when conduction current flows through the electrode. (It is worth remarking that a previous model on potential distribution was based on depletion conditions.[65]) A deeper analysis of these issues will require a more extensive body of experimental evidence than that now available, and is deferred to future studies. At present we can only claim that the evidence from impedance is fully consistent with a drift force distributed throughout the porous structure, but other alternatives cannot be excluded at this point, given that various hypothesis on transport mechanisms give rise to similar relaxation functions, as commented before.

6. Conclusions

Models for the small-signal ac response of porous electrodes can be derived from transport equations and kinetic assumptions, or else they can be postulated directly as a transmission line equivalent circuit. For a given number of distinct elements in the line the relaxation function develops various features in different frequency regimes, which can be classified in terms of the system's characteristic relaxation frequencies. Knowledge of the possible patterns of response is helpful in order to identify the correct model and determine the parameters from the measured impedance spectra. When an element in the line possesses dispersive properties, as is most likely in many types of electrodes made of complex materials, the fractionary exponents manifest themselves in the various regimes of frequency where the corresponding element is dominating the response. The matching of values of the dispersive exponents in different regimes provides evidence for a common origin of diverse features of the spectra. The approach was applied to TiO_2 nanoporous photoelectrodes. We showed that in certain experimental conditions the electrochemical impedance of this system is well described by the coupling of transport along one resistive channel, and an interfacial reaction that must be modeled as a R-CPE circuit. It has been demonstrated that the suggested approach is capable of identifying two characteristic relaxation frequencies in a frequency-resolved measurement on a TiO_2 nanoporous photoelectrode.

Acknowledgment. Discussions with L. M. Peter and P. Salvador are appreciated. This work was supported by la Comisión Interministerial de Ciencia y Tecnología under projects PB98-1045 and MAT98-0342.

References and Notes

(1) Cao, F.; Oskam, G.; Meyer, G. J.; Searson, P. C. *J. Phys. Chem.* **1996**, *100*, 17021.
(2) Zaban, A.; Meier, A.; Gregg, B. A. *J. Phys. Chem. B* **1997**, *101*, 7985.
(3) de Jongh, P. E.; Vanmaekelbergh, D. *J. Phys. Chem. B* **1997**, *101*, 2716.
(4) Dloczik, L.; Ileperuma, O.; Lauerman, I.; Peter, L. M.; Ponomarev, E. A.; Redmond, G.; Shaw, N. J.; Uhlendorf, I. *J. Phys. Chem. B* **1997**, *101*, 10281.
(5) Schlichthröl, G.; Huang, S. Y.; Sprague, J.; Frank, A. J. *J. Phys. Chem. B* **1997**, *101*, 8141.
(6) Huang, S. Y.; Schilchthörl, G.; Nozik, A. J.; Grätzel, M.; Frank, A. J. *J. Phys. Chem. B* **1997**, *101*, 2576.
(7) Franco, G.; Gehring, J.; Peter, L. M.; Ponomarev, E. A.; Uhlendorf, I. *J. Phys. Chem. B* **1999**, *103*, 692.
(8) Franco, G.; Peter, L. M.; Ponomarev, E. A. *Electrochem. Commun.* **1999**, *1*, 61.
(9) Vanmaekelbergh, D.; Iranzo Marín, F.; van de Lagemaat, J. *Ber. Bunsen-Ges. Phys. Chem.* **1996**, *100*, 616.
(10) Ben-Chorin, M.; Möller, F.; Koch, F.; Schirmacher, W.; Eberhard, M. *Phys. Rev. B* **1995**, *51*, 2199.
(11) Parkhutik, V. P.; Matveeva, E. S.; Namavar, F.; Kalcoran, N. *J. Electrochem. Soc.* **1996**, *143*, 3943.
(12) Gelloz, B.; Bsiesy, A. *Appl. Surf. Sci.* **1998**, *135*, 15.
(13) O'Regan, B.; Grätzel, M. *Nature* **1991**, *353*, 737.
(14) Bechinger, C.; Ferrer, S.; Zaban, A.; Sprague, J.; Gregg, B. A. *Nature* **1996**, *383*, 608.
(15) Hens, Z. *J. Phys. Chem. B* **1999**, *103*, 122.
(16) de Levie, R. *Electrochim. Acta* **1963**, *8*, 751.
(17) Raistrick, I. D. *Electrochim. Acta* **1990**, *35*, 1579.
(18) Paasch, G.; Micka, K.; Gersdorf, P. *Electrochim. Acta* **1993**, *38*, 2653.
(19) de Levie, R. In *Advances in Electrochemistry and Electrochemical Engineering*; Delahay, P., Ed.; Interscience: New York, 1967; Vol. 6, p 329.
(20) Keiser, H.; Beccu, K. D.; Gutjahr, M. A. *Electrochim. Acta* **1976**, *21*, 539.
(21) Candy, J.-P.; Fouilloux, P.; Keddam, M.; Takenouti, H. *Electrochim. Acta* **1981**, *26*, 1029.
(22) Cachet, C.; Wiart, R. *Electrochim. Acta* **1984**, *29*, 145.
(23) Gassa, L. M.; Vilche, J. R.; Ebert, M.; Jüttner, K.; Lorenz, W. J. *J. Appl. Electrochem.* **1990**, *20*, 677.
(24) da Silva Pereira, M. I.; Melo, M. J. B. V.; da Costa, F. M. A.; Rosa Nunes, M.; Peter, L. M. *Electrochim. Acta* **1989**, *34*, 663.
(25) Kontturi, K.; Murtomäki, L. *Models Chem.* **1995**, *132*, 191.
(26) Fievet, P.; Mullet, M.; Pagetti, J. *J. Membr. Sci.* **1998**, *149*, 143.
(27) Albery, W. J.; Elliot, C. M.; Mount, A. R. *J. Electroanal. Chem.* **1990**, *288*, 15.
(28) Ren, X.; Pickup, P. G. *J. Phys. Chem.* **1993**, *97*, 5356.
(29) Fletcher, S. *J. Electroanal. Chem.* **1992**, *337*, 127.
(30) Rossberg, K.; Paasch, G.; Dunsch, L.; Ludwig, S. *J. Electroanal. Chem.* **1998**, *443*, 49.
(31) Brumleve, T. R.; Buck, R. P. *J. Electroanal. Chem.* **1981**, *126*, 73.
(32) Vorotyntsev, M. A.; Daikhin, L. I.; Levi, M. D. *J. Electroanal. Chem.* **1994**, *364*, 37.
(33) Buck, R. P.; Mundt, C. *J. Chem. Soc., Faraday Trans.* **1996**, *92*, 3947.
(34) Kramer, M.; Tomkiewicz, M. *J. Electrochem. Soc.* **1984**, *131*, 1283.
(35) Bisquert, J.; Garcia-Belmonte, G.; Fabregat-Santiago, F.; Compte, A. *Electrochem. Commun.* **1999**, *1*, 429.
(36) Albery, W. J.; Mount, A. R. *J. Chem. Soc., Faraday Trans.* **1994**, *90*, 1115.
(37) Ren, X.; Pickup, P. G. *J. Electroanal. Chem.* **1997**, *420*, 251.
(38) Bisquert, J.; Garcia-Belmonte, G.; Bueno, P.; Longo, E.; Bulhões, L. O. S. *J. Electroanal. Chem.* **1998**, *452*, 229.
(39) Bisquert, J.; Garcia-Belmonte, G.; Fabregat-Santiago, F.; Bueno, P. *J. Electroanal. Chem.* **1999**, *475*, 152.
(40) Garcia-Belmonte, G.; Bisquert, J.; Fabregat-Santiago, F.; Yamashita, M.; Pereira, E. C. *Ionics* **1999**, *5*, 44.
(41) Mott, N. F.; Davies, E. A. *Electronic Processes in Non-Crystalline Materials*; Clarendon Press: Oxford, UK, 1979.
(42) Dyre, J. C. *J. Appl. Phys.* **1988**, *64*, 2456.
(43) Pajkossy, T. *J. Electroanal. Chem.* **1994**, *364*, 111.
(44) Scheider, W. *J. Phys. Chem.* **1975**, *79*, 127.
(45) Láng, G.; Heusler, K. E. *J. Electroanal. Chem.* **1998**, *457*, 257.
(46) McCann, J. F.; Badwal, S. P. S. *J. Electrochem. Soc.* **1982**, *129*, 551.
(47) Goossens, A.; Schoonman, J. *J. Electrochem. Soc.* **1992**, *139*, 893.
(48) Oskam, G.; Vanmaekelbergh, D.; Kelly, J. J. *J. Electroanal. Chem.* **1991**, *315*, 65.
(49) Le Mehaute, A.; Crepy, G. *Solid State Ionics* **1983**, *9*−*10*, 17.
(50) Le Mehaute, A. *J. Stat. Phys.* **1984**, *36*, 665.
(51) Epelboin, I.; Keddam, M. *J. Electrochem. Soc.* **1970**, *117*, 1052.
(52) de Levie, R. *J. Electroanal. Chem.* **1990**, *281*, 1.
(53) Barbé, C. J.; Arendse, F.; Comte, P.; Jirousek, M.; Lezmann, F.; Shklover, V.; Grätzel, M. *J. Am. Ceram. Soc.* **1997**, *80*, 3157.
(54) Jamnik, J.; Maier, J.; Pejovnik, S. *Electrochim. Acta* **1996**, *41*, 1011.
(55) Ohmori, T.; Kimura, T.; Masuda, H. *J. Electrochem. Soc.* **1997**, *144*, 1286.
(56) Macdonald, J. R. *Impedance Spectroscopy*; John Wiley and Sons: New York, 1987; p 122.
(57) Cabanel, R.; Barral, G.; Diard, J.-P.; Le Gorrec, B.; Montella, C. *J. Appl. Electrochem.* **1993**, *23*, 93.

(58) Gabrielli, C.; Takenoutti, H.; Haas, O.; Tsukada, A. *J. Electroanal. Chem.* **1991**, *302*, 59.
(59) Nguyen, P. H.; Paasch, G. *J. Electroanal. Chem.* **1999**, *460*, 63.
(60) Moya, A. A.; Horno, J. *J. Electroanal. Chem.* **1998**, *459*, 145.
(61) Bisquert, J.; Compte, A., manuscript in preparation.
(62) Lemon, B. I.; Hupp, J. T. *J. Phys. Chem.* **1996**, *100*, 14578.
(63) Boschloo, G. K.; Goossens, A.; Schoonman, J. *J. Electrochem. Soc.* **1997**, *144*, 1311.
(64) Södergren, S.; Hagfeldt, A.; Olsson, J.; Lindquist, S. E. *J. Phys. Chem.* **1994**, *98*, 5552.
(65) Bisquert, J.; Garcia-Belmonte, G.; Fabregat-Santiago, F. *J. Solid State Electrochem.* **1999**, *3*, 337.